Electrical behaviour, characteristics and properties of anodic aluminium oxide films coloured by nickel electrodeposition

Laurent Arurault · Gaël Zamora · Virginie Vilar ·
Peter Winterton · René Bes

Abstract Porous anodic films on 1050 aluminium substrate were coloured by AC electrodeposition of nickel. Several experiments were performed at different deposition voltages and nickel concentrations in the electrolyte in order to correlate the applied electrical power to the electrical behaviour, as well as the characteristics and properties of the coatings. The content of nickel inside the coatings reached 1.67 g/m^2, depending on the experimental conditions. According to the applied AC voltage in comparison with the threshold voltage U_t, the coating either acted only as a capacitor when $U < U_t$ and, when $U > U_t$, the behaviour during the anodic and cathodic parts of the power sine wave was different. In particular, due to the semi-conducting characteristics of the barrier layer, additional oxidation of the aluminium substrate occurred during the anodic part of the electrical signal, whilst metal deposition (and solvent reduction) occurred during the cathodic part; these mechanisms correspond to the blocked and pass directions of the barrier layer/electrolyte junction, respectively.

Introduction

Although the principle of metal electrodeposition in porous anodic films on aluminium alloys was reported in 1936 in Italy [1, 2] and 1940 in Norway [1, 2], the industrial advent of the process really occurred in Japan in the 1960s with Asada's works [1] on the preparation of coloured coatings. In this case, the electrodeposition process is known as electrocolouring: the two main fields of application are coloured coatings for architecture and selective surfaces for solar energy storage and conversion.

Various metals or alloys have been tested (Table 1) giving a large range of colours, depending on the experimental parameters, especially the initial anodizing electrolyte influencing the characteristics of the anodic films, the colouring electrolyte composition, as well as the type of metal and how much was actually deposited [3–6]. Lee et al. [7] also showed the importance of the alloy substrate and the pre-treatment used on it in nickel electrocolouring. However, it is important to note that industrial developments, but also academic studies, mainly focus solely on applications, apart from Goad and Moskovits [8] who proposed a model to explain colour phenomena.

To prepare solar absorbers, the thermo-optical properties required are total absorptivity of solar radiation (0.2–2.5 μm) higher than 90% and total hemispherical emissivity, in the infrared wavelength range (2.5–25 μm), lower than 20%. The best results are usually achieved with 'black' colours, obtained by the electrodeposition of nickel [9–17] or more rarely cobalt [18, 19].

The deposition electrolyte is usually a sulphate solution of the metal to be deposited in acidic conditions, or a mixture of sulphate and chloride with Watts electrolyte [20] for nickel deposition. However, other compounds are sometimes added to the electrolyte to increase conductivity: especially $(NH_4)_2SO_4$, $Al_2(SO_4)_3$ and $MgSO_4$ [16, 21] and on occasions organic compounds are included as complexing agents [22–24]. The counter-

L. Arurault (✉) · G. Zamora · V. Vilar · R. Bes
CIRIMAT, UPS/INPT/CNRS, LCMIE, Université de Toulouse,
Bat 2R1, 118 Route de Narbonne, 31062 Toulouse Cedex 9,
France
e-mail: arurault@chimie.ups-tlse.fr

P. Winterton
Université de Toulouse, Bat 4A, 118 Route de Narbonne,
31062 Toulouse Cedex 9, France

Table 1 Correlation between the nature of the metal deposited and the colour it confers

Metal	Colour
Copper [8, 22, 40, 41]	From pink to dark red
Bismuth [42]	Blue
Iron [43]	From buff to dark bronze
Tin [9, 25, 32, 39, 44]	Dark blue
Nickel [1, 7–17, 45]	From black to bronze
Tin–nickel alloy [46]	Blue-violet
	Blue
	Grey
	Yellow-green
	Yellow–red
Lead [47]	From buff to dark bronze
Silver [8]	Yellow
Molybdenum [8]	Yellow
Gold [8]	Mauve
Zinc [48]	Maroon
	Brown
	Green
	Grey

electrode is usually made of the metal to be deposited, in order to maintain the cationic concentration constant in the electrolyte; but graphite [8], platinum [25] or steel [2] are also sometimes used. Electrodeposition is usually performed at ambient temperature, and only exceptionally at higher temperatures, i.e. 30 °C [12] and 50 °C [20].

Considering the usual diameter (from 5 to 500 nm) of the pores in anodic films [26], the deposition of metal requires cations to be constantly transported into the pores. As a consequence, when DC is used, electrodeposition cannot occur [9], except on the very surface of the sample at the highest values of current/voltage. Usually, metal electrodeposition in the pores of the anodic films is performed using alternating voltage (or sometimes alternating current [7]) at 50 or 60 Hz, although pulsed signals are also used [27] especially by Zemanova et al. [23, 24, 28, 29]. But the choice how the electrical power is applied affects the microshape of the deposited metal [30]. In these AC or pulsed conditions, the reaction mechanisms remain to be clarified from the point of view of the electrochemical process and the material changes brought about.

The aim of the present work was to study electrocolouring by nickel deposition, using alternating voltage, in porous anodic films on aluminium substrate, and especially to correlate the power applied to the electrical behaviour, as well as the characteristics and colour properties of the coatings.

Experimental

Preparation process

The aluminium substrate was a 1050 A alloy (99.5% Al). All chemicals used were of analytical grade (Prolabo) and aqueous electrolyte solutions were made up using deionised water.

The preparation process involved three main successive steps: pre-treatment of the surface, anodizing and electrochemical deposition of nickel.

Alloy sheet ($60 \times 40 \times 1$ mm) was degreased for 1 min in an aqueous alkaline bath containing NaOH (5 g/L), $Na_2CO_3.6H_2O$ (5 g/L), $Na_3PO_4.12H_2O$ (10 g/L), $Na_2SiO_3.5H_2O$ (1 g/L) and sodium gluconate ($NaC_6H_{11}O_7$, 10 g/L), then etched in aqueous NaOH (25 g/L) for 1 min and neutralized in aqueous HNO_3 (20%v/v) for 2 min. Each step was conducted at ambient temperature, and the samples were immediately rinsed in distilled water.

The aluminium sheet was then used as anode and a lead plate ($3 \times 40 \times 40$ mm) as counter-electrode in the electrochemical cell thermostatted at 25 °C. The anodisation was run for 15 min (900 s) in the potentiostatic mode (U_a kept at 20 V) using a mixed solution (pH = 0.5) of H_2SO_4 (40 g/L) and H_3BO_3 (10 g/L) at 25 °C. The addition of boric acid as a modifier in the sulphuric acid anodising bath is known to improve the properties of the anodic films, especially the microhardness and the thickness [26, 31].

Nickel electrodeposition in the prepared porous anodic films was carried out in an electrochemical cell thermostatted at 25 ± 2 °C, using a nickel plate ($60 \times 40 \times 1$ mm) as counter-electrode, located parallel at 4 cm from the sample. The deposition bath used was previously developed by Salmi [10, 14] but using phosphoric acid as anodising electrolyte. The deposition electrolyte was made up of $NiSO_4 \cdot 6H_2O$ (30 g/L), H_3BO_3 (20 g/L), $MgSO_4 \cdot 7H_2O$ (20 g/L) and $(NH_4)_2SO_4$ (20 g/L). Before beginning metal deposition, the sample was dipped in the electrolyte for 30 s at a voltage which corresponds to an open-current circuit. Electrochemical deposition was then performed using alternating voltage (Blanc Electronique SA supply, type EA-4036), at a frequency of 50 Hz, the applied effective voltage varying from 5 to 30 V, whilst an oscilloscope recorded the voltage and current waveforms. Usual deposition conditions were an effective voltage of 10 V and a duration of 10 min (600 s). After treatment, the specimens were immediately removed from the electrolyte and washed with de-ionised water.

Microscopic and chemical analyses

Chemical analysis of the deposited metal was performed, after acid dissolution of the anodic film, by inductively

coupled plasma (ICP) with a Jobin–Yvon 24 spectrophotometer. For this purpose, a disc (diameter = 14 mm) was cut in the sample and placed in an acidic solution (10 mL of HNO_3 0.1 M) under vigorous mixing until the coating had completely dissolved. The solution was then made up to a final volume of 50 mL with deionised water. Finally, the concentration obtained by ICP analysis was converted to nickel content per surface area (mg/m^2).

Transmission electron microscopy (TEM JEOL 200CX) was used to determine the morphology and the characteristics of the porous anodic film, i.e. the pore density (ρ), the pore diameter (d_p), the thickness of the porous layer (e_p) and the thickness of the barrier (or compact) layer (e_b). For the TEM top views, a disc (diameter = 14 mm) was cut in the sample. The sample preparation procedure was then: mechanical polishing performed on the back of the disc, ultrasound cutting of a smaller disc (diameter = 3 mm), mechanical hollowing on the back of the disc; thinning and drilling of a hole using precision ion polishing system (PIPS) to enable observation. For the TEM cross-sectional views, the sample was cut into strips (width 1 mm); the sample preparation procedure was then: gluing with epoxy glue of two strips face to face, potting in a brass tube (diameter = 3 mm), cutting the tube in thin strips, mechanical hollowing thinning and drilling a hole using PIPS to enable observation.

The colour of the coating was evaluated, using a spectrocolorimeter (Minolta 2500d), through three parameters $L*$, $a*$, $b*$ corresponding to its coordinates in colorimetric LAB space, defined by the International Commission on Illumination (CIE). $L*$ corresponds to the brightness (0: black; 100: white), $a*$ describes the colour from green to red (−60 to +60, respectively) and $b*$ from blue to yellow (−60 to +60, respectively). Black ideally has the following coordinates: $L* = 0$; $a* = 0$; $b* = 0$.

Results and discussion

Electrical behaviour during the deposition process

Experimental results

The impact of deposition voltage was studied during nickel deposition (5 s) in an anodic film (20 V, 900 s) using different effective voltages from 3 to 25 V (Fig. 1). Figure 2 shows the maximum anodic current density $(J_{max})_a$ and cathodic current density $(|J_{max}|)_c$ as a function of effective deposition voltage. Three voltage domains are highlighted.

When $U_{eff} = 3$, 7 or 9 V, the values of $(J_{max})_a$ and $(|J_{max}|)_c$ are almost equal. Furthermore, in this voltage range, maximum current density was proportional to

effective voltage. When $U_{eff} > 9$ V, maximum current densities $(J_{max})_a$ and $(|J_{max}|)_c$ rose linearly as a function of the voltage to a maximum of about $U_{eff} = 15$ V. Beyond this $(J_{max})_a$ remained stationary whereas $(|J_{max}|)_c$ decreased.

Moreover, the extrapolation of intermediate linear parts (between 9 and 15 V) to $J_{max} = 0$ allowed us to accurately define the deposition threshold potential U_t which, in our conditions, was near 8 V.

Deposition voltage also has a significant impact when the current density wave is compared to the applied voltage waveform. In fact, when the voltage was below the threshold voltage ($U < U_t$), a constant phase difference always appeared between the voltage wave and the current density wave (Fig. 3). Beyond the threshold voltage, a phase difference occurred between the intensity and the voltage on the anodic part of the signals whereas the two cathodic parts were perfectly in phase (Fig. 4).

Discussion

The impact of voltage on the impregnation process is underlined: depending on whether this value is above or below the threshold voltage U_t, reaction mechanisms are obviously different.

In the lowest voltage range ($U < U_t$; e.g. $U < 8$ V), maximum current densities were proportional to the effective voltage and were equal
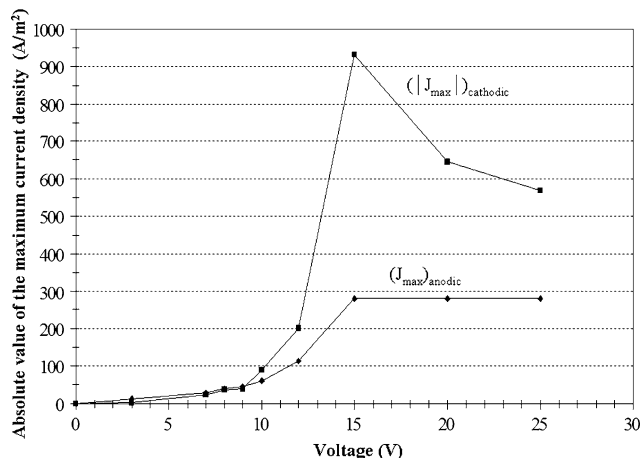
$$(J_{max})_a = |(J_{max})_c|$$

The phase difference between the voltage wave and the current density wave was constant in both anodic and cathodic parts. As previously mentioned by Sato and Sakai [1], this resembles the usual behaviour of a capacitor. In this case, the deposition process would induce charge and discharge cycles depending on the alternating anodic and cathodic phases, respectively. In this case, when an alternating voltage is applied ($u = U_0 \sin(\varpi t)$, where ϖ is the imposed signal pulse and f its frequency: $\varpi = 2 \cdot \pi \cdot f$ with $f = 50$ Hz), the intensity response is also an alternating waveform ($i = I_0 \sin(\varpi t + \phi)$) but showing a phase difference ϕ.

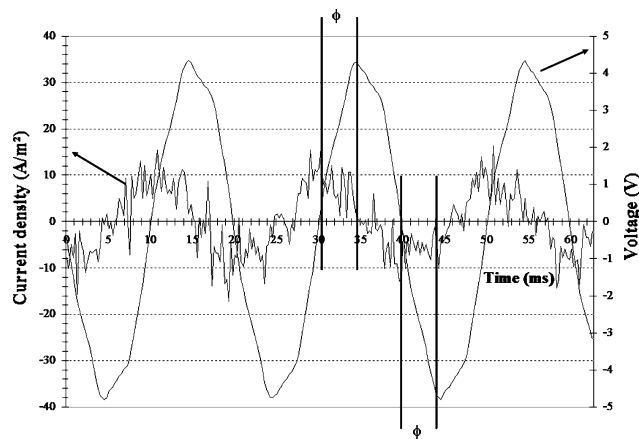At higher voltages ($U > U_t$) the experimental results showed that

– the anodic parts of voltage and current density were out of phase, whereas the corresponding cathodic parts were in phase ($\phi = 0$);
– the current density wave was not totally symmetrical and changed during the first 420 s (7 min);
– this electrical behaviour was confirmed even when there were no nickel cations in the electrolytic bath, i.e. when the electrolyte includes only boric acid, ammonium sulphate and magnesium sulphate.
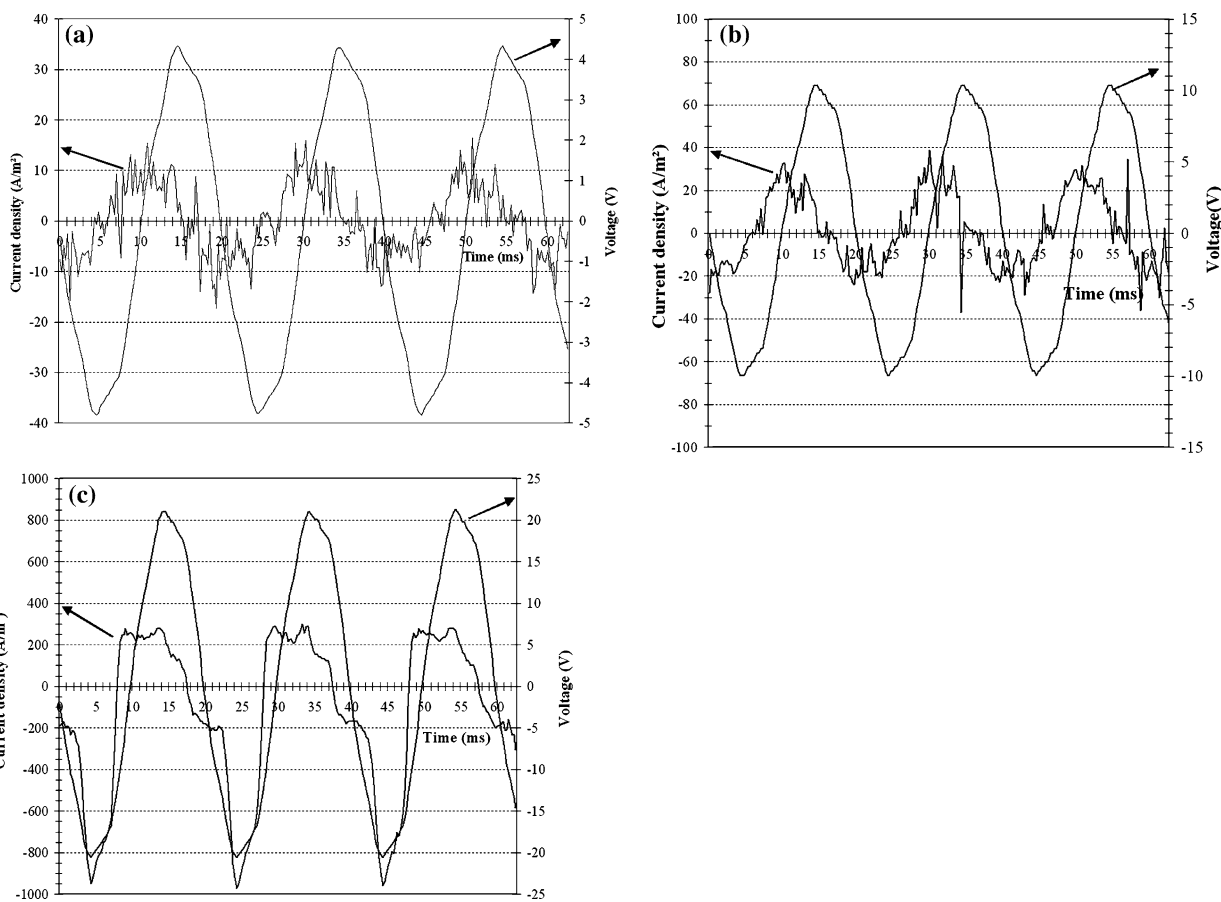
Fig. 4 Phase difference between voltage wave and current density wave during nickel deposition (25 V, 5 s) in a sulphuric–boric anodic film (20 V, 900 s)

Fig. 5 TEM cross-sectional view of a sulphuric–boric anodic film (20 V, 900 s) including nickel (10 V, 600 s, 30 g/L)

deposition. Beyond 420 s, i.e. at the end of deposition, or using an electrolyte without metal cations, the reaction is thought to correspond to solvent reduction [32] with hydrogen evolution.
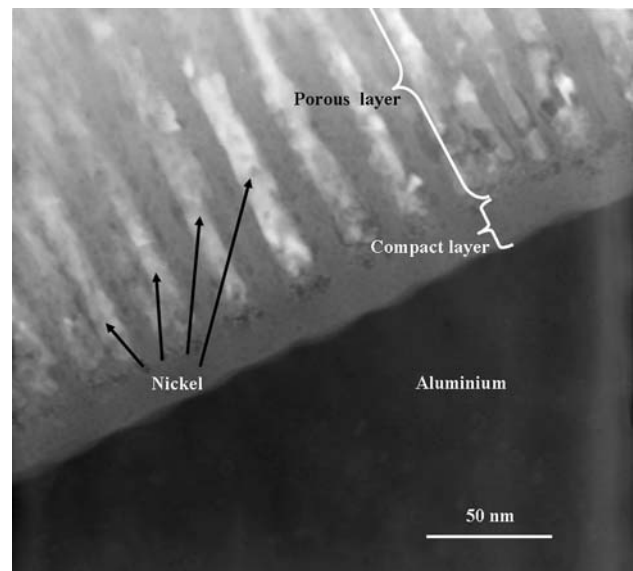
The end of deposition, which occurs after a few minutes, seems to result from the simultaneous evolution of both the anodic and cathodic parts of the signal as function of deposition duration. According to previous studies [12, 25], current density decrease could be a consequence of an increase in anodic film resistance, due to an increase of the barrier layer thickness by complementary re-anodizing during the anodic part; this phenomenon occurs when the anodizing voltage is lower than the deposition alternating voltage [32]. Nevertheless, previous works [25, 32] have specified that this additional anodisation occurs fastest in the first 15 s of the deposition step whereas here the evolution of the anodic and cathodic parts of the signal continues for up to 420 s. However, this remains plausible because additional growth of the barrier layer was experimentally observed at the end of the deposition step under alternating voltage.

Threshold voltage and coating characteristics

Experimental results

Figure 5 and Table 2 show the morphological characteristics of the anodic films before and after deposition, as well as the metal content (γ) in the pores.

Pore density and diameter did not vary significantly with metal insertion in the anodic film under conditions of alternating voltage. On the contrary, the porous layer thickness decreased whilst the barrier layer thickness significantly increased, confirming the hypothesis of additional

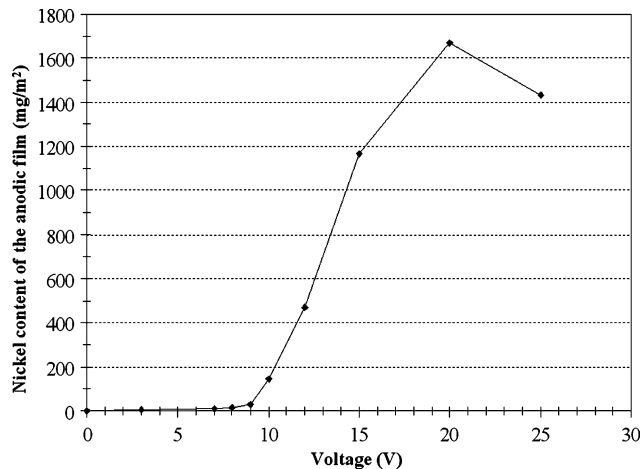anodisation of the substrate during the anodic part of the alternating signal.

Furthermore, the metal content of the anodic film was recorded (Fig. 6) as a function of the effective voltage (3–25 V) for a fixed duration (600 s), and the impact of nickel concentration in the electrolyte on the amount of metal deposited was also studied (Fig. 7) for nickel deposition under fixed voltage and for a given duration (10 V, 600 s). The metal content was varied from 0 to 1.65 g/m² according to the experimental conditions of deposition. These values are in accordance with data from the literature [13, 29, 33] indicating nickel contents from 0.5 to 1.4 g/m² depending on the operational conditions of metal deposition.

Figure 6 clearly illustrates that deposition occurs above a threshold voltage, here about 8–9 V. For example, at 12 V the metal content was about 90 μg/cm² (i.e. 900 mg/m²) in anodic films obtained in phosphoric acid electrolyte [10], whilst it is about 500 mg/m² in the present study. This difference is partially explained by the change of void volume in the different types of anodic films: the porosity of anodic films obtained in sulphuric–boric acids is significantly lower (about 4%) than that of anodic films (about 37%) prepared with phosphoric acid [34].

A second threshold voltage was also observed about 17–18 V. From this second value, the quantity of metal deposited seems to be independent of the effective voltage. Here we reached about 1.4 g/m², whilst Salmi [10, 14] reported a maximum value of about 0.8 g/m² for 10 V AC and 1.2 g/m² at 15 V AC. At the highest voltages, deposition was uneven.

Table 2 Characteristics of the anodic porous films before and after nickel deposition (10 V, 600 s)

Anodisation electrolyte	Thickness of the porous layer (μm)	Average pore diameter (nm)	Thickness of the barrier layer (nm)	Average height of the metal deposited (nm)	γ (mg/m^2) ($\pm 5\%$)
Mixed sulphuric–boric acid solution					
Before deposition	6.1 ± 0.2	10 ± 4	19 ± 3	–	–
After deposition	2.0 ± 0.1	8 ± 3	27 ± 3	500 ± 100	147

Fig. 6 Metal content in sulphuric–boric anodic film (20 V, 900 s) versus effective voltage (3-25 V) for a fixed duration (600 s)
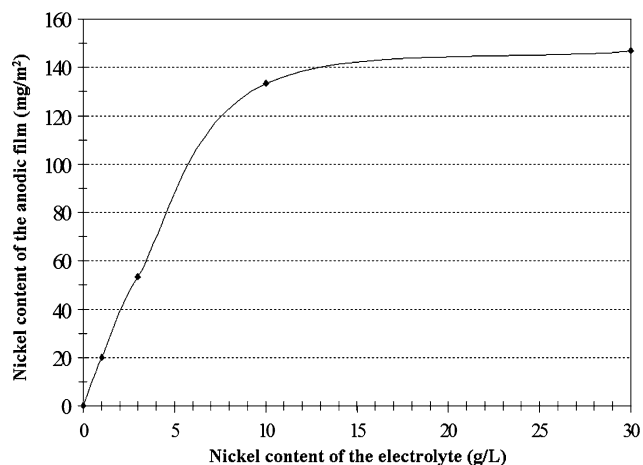
Fig. 7 Influence of nickel concentration (0-30 g L^{-1}) in the electrolyte on the metal content in the anodic film in the case of nickel deposition (10 V, 600 s)

Moreover, the influence of electrolyte nickel concentration on the quantity of metal deposited was studied in the range 0–30 g L^{-1}, keeping the electrolyte ionic strength and conductivity similar. Figure 7 shows a plot similar to one previously obtained [10] for identical metal impreg-nation (up to 12 g L^{-1}) on phosphoric anodic films. In the 0–8 g L^{-1} concentration range, the amount of metal deposited seems to be directly proportional to the electrolyte concentration but from 10 g L^{-1}, it tends to remain constant at about 0.147 g m^{-2}.

Discussion

The threshold voltage is an essential parameter for electrocolouring of porous anodic films. It corresponds to the beginning of metal deposition at the bottom of the pores, i.e. in contact with the barrier layer [35, 36]. Previous results [29, 34, 37, 38] have proved that the barrier layer is not in fact an insulator but that it acts as an n-type semi-conductor.

Considering the aluminium alloy/barrier layer/electrolyte system, the semi-conductor (SC) could be in majority carrier depletion or accumulation conditions [38]. In the event of depletion, carrier number decreases in the neighbourhood of the semi-conductor interface with the electrolyte. From the point of view of the charges at the junction, the semi-conductor has a lower n-type character in the thickness of space charge than in the rest of the material, whereas the electrolyte has a negatively charged Helmholtz layer. So a junction potential E_j is created at the SC/electrolyte interface.

Now, if the electrode is polarized as a cathode, electron flow will exist at the junction which reduces the existing junction field and allows the conduction of current if $E_{applied}$ is higher than E_j. This first configuration corresponds to the polarization in the pass-direction or direct direction at the SC/electrolyte junction. In this case, the junction potential could represent the threshold potential above which solvent reduction or metal deposition is possible.

In contrast, if the electrode is polarized as an anode, charge carrier numbers will still decrease at the interface, so the junction potential will rise. This second electrical configuration corresponds to the blocked-direction of the SC/electrolyte junction, which forbids electrical conduction at this interface. This leads to further aluminium oxidation at the aluminium/substrate interface or to a breakdown of the dielectric at higher voltages.

Coating properties

Experimental results

The colour of the coatings was studied as a function of the experimental conditions of the deposition process, especially the deposition voltage (Table 3), the nickel concentration in the electrolyte (Table 4), as well as directly the metal content of the anodic films (Fig. 8).

For an effective voltage lower than the threshold voltage ($U < 9$ V) (Table 3), the colour is similar to that of an untreated sample, i.e. metallic grey. At higher values, deposition becomes effective and the coating acquires a brown colour, becoming darker at increasing voltages. In particular at 15 V, the sample obtains a homogeneous dark black colour ($L^* = 21.18$; $a^* = 0.32$; $b^* = -0.15$) but it becomes uneven at higher voltages.

Table 4 shows that the colour remains grey at the lowest nickel concentration (1 g/L). From 3 g/L, the coating has a buff colour, progressively becoming light brown at 30 g L^{-1}.

Discussion

Finally, in the 0–1.2 g/m^2 concentration range, it appears that the brightness (L^*) is directly correlated to the content of metal inside the anodic film (Fig. 8).

$$L^* = 21 + 69 \cdot \exp(-0.004 \cdot m_{Ni}) \quad (1)$$

It is notable that for all samples, especially for the darkest ones (15 V, 30 g NiSO$_4$/L, 1167 mg.m^{-2}), the brightness L^* remained higher than 21. This could be due to the significant influence of the aluminium metal substrate through the relatively low thickness of the coloured coating, i.e. 6 μm. But similar results were also
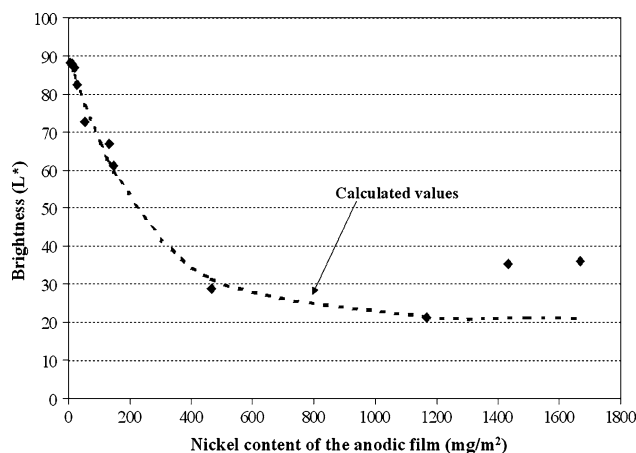

Fig. 8 Correlation between the brightness L* and the nickel content in the anodic films (20 V, 900 s)

reported by Akolkar et al. [39] working on tin deposition, showing that the brightness decreases as the tin content increases.

Conclusion

Coloured anodic films were prepared by electrodeposition of nickel using AC voltage. Several experiments were performed in different conditions (deposition voltage and nickel concentration) to study and correlate the applied electrical power to the electrical behaviour, characteristics and properties of the coatings. The results showed that the metal content varies up to 1.67 g/m^2 according to the operational conditions.

In particular, the voltage impact on the final material clearly depends on its value in comparison with the threshold voltage U_t. For lower values, the coating acts

Table 3 Colour changes of anodic films including nickel versus the effective deposition voltage of nickel electrocolouring (NiSO$_4$ = 30 g/L, 600 s)

Effective voltage (V)	3	7	9	10	12	15	20	25
γ (mg m^{-2})	6.7	10	27	147	467	1167	1667	1433
Coordinates in the lab space								
L^*	88.16	87.93	82.55	61.21	28.80	21.18	36.11	35.32
a^*	−0.39	−0.35	0.56	3.25	5.76	0.32	1.02	0.45
b^*	0.13	0.29	4.76	11.52	8.16	−0.15	4.08	2.65

Table 4 Colour changes of the anodic films including nickel versus the nickel sulphate concentration in the electrocolouring (10 V, 600 s) electrolyte

Weight concentration of nickel sulphate (g/L)	1	3	10	30
Molar concentration of nickel sulphate (mol/L)	0.004	0.011	0.038	0.110
γ (mg m^{-2})	20	53	133	147
Coordinates in the Lab space				
L^*	86.96	72.58	66.82	61.21
a^*	0.11	1.58	2.71	3.25
b^*	0.95	5.27	11.19	11.52

only as a capacitor, whilst at higher voltages the current waveform evolves in its anodic and cathodic parts as a function of the deposition duration. This phenomenon was explained by the additional growth of the barrier layer. Due to the semi-conducting characteristics of the barrier layer, further oxidation of the aluminium substrate occurs during the anodic part of the sign wave, whilst metal deposition (and solvent reduction) occurs during the cathodic part; these mechanisms correspond to the blocked and pass directions of the barrier layer/electrolyte semi-conductor junction, respectively.

References

1. Sato T, Sakai S (1979) Trans Inst Met Finish 57:43
2. Wernick S, Pinner R, Sheasby PG (1987) The surface treatment and finishing of aluminium and its alloys, vol I, 5th edn. ASM Intern. & Finishing Pub. Ed, Teddington, England
3. Kawaguchi T, Ono S, Sato T, Masuko N (1990) J Surf Finish Soc Jpn 41:690
4. Hsieh SAK (1981) Met Finish 79:21
5. Asada T (1977) US Patent 4,022,671
6. Anicai L, Meghea A, Sirean C, Dima L (1995) Mater Sci Forum 185–188:489
7. Lee JH, Lee DN, Kang IK (1978) Plat Surf Finish 1:40
8. Goad DGW, Moskovits M (1978) J Appl Phys 49:2929
9. Kallithrakas-Kontos N, Moshohoritou R, Ninni V, Tsangaraki-Kaplanoglou I (1998) Thin Solid Films 326:166
10. Salmi J (1999) PhD University Paul Sabatier, Toulouse, France
11. Li L (2000) Sol Energy Mater Sol Cells 64:279
12. Shaffei MF, Abd El-Rehim SS, Shaaban NA, Huisen HS (2001) Renew Energy 23:489
13. Granqvist CG, Andersson A, Hunderi O (1979) Appl Phys Lett 35:268
14. Salmi J, Bonino JP, Bes RS (2000) J Mater Sci 35:1347. doi:10.1023/A:1004773821962
15. Kumar SN, Malhotra LK, Chopra KL (1983) Sol Energy Mater 7:439
16. Othonos A, Nestoros M, Palmerio D, Christofides C, Bes RS, Traverse JP (1998) Sol Energy Mater Sol Cells 51:171
17. Yu-Wen Z, Han-Fen H, Bao-Ying Z (1985) Int J Sol Energy 3:271
18. Nahar NH, Mo GH, Ignatiev A (1986) Sol Energy Mater 14:129
19. Nahar NH, Mo GH, Ignatiev A (1989) Thin Solid Films 172:19
20. Fukuda Y, Fukushima T (1982) J Met Finish Soc 33:50
21. Wäckelgard E (1998) Sol Energy Mater Sol Cells 54:171
22. Jagminas A, Kuzmarskyte J, Niaura G (2002) Appl Surf Sci 201:129
23. Zemanova M, Chovancova M, Blaho P, Usak E, Valtyni J (2008) Trans Inst Met Finish 86:109
24. Zemanova M, Gal M, Chovancova M (2009) Trans Inst Met Finish 87:97
25. Itoi Y, Hasumi A, Sato E, Tachihara K (1980) Electrochim Acta 25:1297
26. Arurault L (2008) Trans Inst Met Finish 86:51
27. Arurault L, Salmi J, Bes RS (2004) Sol Energy Mater Sol Cells 82:447
28. Zemanova M, Chovancova M, Galikova Z, Krivosik P (2008) Renew Energy 33:2303
29. Zemanova M, Chovancova M, Krivosik P (2009) Chem Pap 63:62
30. Wazwaz A, Bes RS, Abed-Rabbo A, Mastai Y (2003) Int J Sustain Energy 23:121
31. Shih HH, Tzou SL (2000) Surf Coat Technol 124:278
32. Tsangaraki-Kaplanoglou I, Theohari S, Dimogerontakis Th, Kallithrakas-Kontos N, Wang YM, Kuo HH, Kia S (2006) Surf Coat Technol 201:2749
33. Anderson A, Hunderi O, Granqvist CG (1980) J Appl Phys 51:754
34. Zamora G (2005) PhD University Paul Sabatier, Toulouse, France
35. Arurault L, Zamora G, Bes RS (2007) Galvano-Organo Trait Surf 767:40 (in French)
36. Arurault L, Bes RS (2003) Adv Eng Mater 5:433
37. Arurault L, Zamora G, Bes RS (2006) ATB Metall 45:306
38. Vrublevsky I, Jagminas A, Schreckenbach J, Goedel WA (2007) Appl Surf Sci 253:4680
39. Akolkar R, Wang YM, Kuo HH (2007) J Appl Electrochem 37:291
40. Pastore G, Montes S, Paez M, Zagal JH (1989) Thin Solid Films 173:299
41. Shimizu K, Habazaki H, Skeldon P, Thompson GE, Wood GC (1999) Surf Int Anal 27:1046
42. Peng Y, Qin DH, Zhou RJ, Li HL (2000) Mater Sci Eng B77:246
43. Yongqing S (2000) Met Finish 12:61
44. Tsangaraki-Kaplanoglou I, Theohari S, Dimogerontakis Th, Kallithrakas-Kontos N, Wang YM, Kuo HH, Kia S (2006) Surf Coat Technol 200:3969
45. Carlsson B, Möller K, Frei U, Brunold S, Köhl M (2000) Sol Energy Mater Sol Cells 61:223
46. Kawai S, Yamamuro M (1997) Plat Surf Finish 5:116
47. Yongqing S, Zihe M, Jiaqiang G, Yuan Y (1999) Met Finish 12:8
48. Dasquet JP (1999) PhD thesis, University Paul Sabatier, Toulouse, France